Using the Topographic Wetness Index (TWI) to Identify Landslide Risks to Rural Water Supplies and Sanitation in the Indian Himalayan

Swati Punyal[1], Dr. Parveen Kumar[2]

Abstract

Rural water supply and sanitation facilities across the Himalayan region are frequently destroyed or contaminated by landslides. Despite this, WASH (Water, Sanitation, and Hygiene) infrastructure is rarely considered in hazard assessments. This study demonstrates that the Topographic Wetness Index (TWI) can effectively identify landslide-vulnerable water sources in data-scarce mountain environments. Using landslide inventory from the Bhukosh portal for Solan district in Himachal Pradesh, India, logistic regression models and quadratic discriminant functions were employed to calculate TWI, rainfall and Stream Power Index (SPI). Results indicated that TWI explained 75.7% of the variation in landslide incidence, which is greater than yearly rainfall (R^2 = 0.6598) and far greater than the SPI model (R^2 = 0.5094). The high predictive value of TWI was confirmed by logistic regression (AUC = 0.872) with an average AUC (based on five-fold cross-validation) of 0.865 (±0.021). Overlay mapping indicates that high-TWI (TWI > 6.2) areas have the greatest susceptibility to landslides; 78% of the springs and 71% of the shallow wells are in this zone. The integrated software of the full research was under $500 (approximately ₹43,000) and this satellite-based data is free and can be used by district WASH departments to replicate the software. The data deposited in Zenodo show that after a significant landslide in August 2023, the turbidity in the impacted springs increased by 359%, and the coliform counts jumped from less than 10 to more than 500 MPN/100 mL. Simple, low-cost interventions identified to be effective in reducing risk were cleaning of drains around springs, diversion of run-off, moving latrines away from high TWI areas, and implementing post-landslide water quality emergency procedures. TWI mapping is an approach that can be implemented realistically and reproducibly for climate-resilient water, sanitation, and hygiene (WASH) planning in the Himalayan regions.

[1]PhD Scholar, Department of Architecture, DCRUST, Murthal, spunyal@gmail.com
[2]Professor, Department of Architecture, DCRUST, Murthal, parveenkumar.arch@dcrustm.org

Keywords: Annual Rainfall, Landslides, Water Supplies, Sanitation, Himalayas, Climate Resilience, Topographic Wetness Index (TWI).

1. Introduction

Clean drinking water and better sanitation are basic human rights (United Nations General Assembly, 2010). Goal 6 (Sanitation and Clean Water) and Goal 13 (Climate Action) are both directly aided by this study. Despite all this, many populations in rural areas of the Hindu Kush Himalaya rely on water sources that are highly vulnerable to landslides, such as springs, shallow wells, and gravity-fed piped water infrastructure. Every monsoon, water intakes are destroyed, wellheads are covered in silt and feces from non-functioning latrines, and pipelines are broken, rendering springs unusable. The Indian Himalaya experiences around 15% of the total rain-induced landslides on the earth's surface. Whole villages in Nepal were without access to potable water for weeks after the 2015 Gorkha earthquake due to landslides. The only supply of water for two hundred and thirty homes in Nepal's Chhabispathibhera Rural Municipality was destroyed in a landslide that occurred in September 2024 (INSEC, 2024).

However, the condition is serious in Indian Himalaya particularly in the parts that are protected by weak and clayey Siwalik geology like Solan in Himachal Pradesh. The shear failure of Siwalik rocks invariably occurs within the clayey parts of clay shales which are the weakest part of the rocks (Bhandari & Dhakal, 2018). In this area, the most frequent type of landslide is a saturation driven landslide, rather than stream erosion. This water then moistens the soil and raises the pore pressure. In these converging hollows, both traditional well-digging and spring-emergence take place.

Topographic Wetness Index (TWI) is an indicator of the expected concentration of water as a function of the topography. In this article, this was addressed by comparing this to two other hydrological predictors: rainfall and the Stream Power Index (SPI). Analysis of the recent studies in Uttarakhand indicated that TWI is a crucial parameter to consider when evaluating the risk of a landslide.A recent study in Uttarakhand revealed that TWI is a significant indicator for landslide risk assessment (Bharadwaj & Sarkar, 2024). The Solan area was used as a case study to investigate three research questions:

1. How well do TWI, rainfall, and SPI discriminate landslides from stable terrain?
2. What proportion of water sources and sanitation facilities lie in high-risk zones?
3. What low-cost interventions can district WASH departments implement?

2. Study area: Solan district, Himachal Pradesh, India

Covering over 1,936 km², the Solan district is located in the Lesser Himalayan zone of Himachal Pradesh (30°45′-31°15′ N, 76°45′-77°15′ E) (Figure 1). Slopes were frequently in excess of 30° and elevations ranged from 300 m in the southwest to nearly 2,100 m in the northeast.

Under the district are sediments of the Siwalik Group consisting of alternate sandstones, siltstones, claystones and conglomerates, formed during the Upper Miocene and Pleistocene. The monsoon creates perched water levels in the clayey strata, which results in limited permeability and landslides driven by saturation. The centred log-ratio of silt/clay fraction and mean log of silt/clay fraction of the soil has been found to cause landslide initiation (Bhandari and Dhakal, 2020).

More over three quarters of the rain (900-1,500 mm) that falls each year falls during the southwest monsoon (June–September). A study carried out in the Uttarkashi region identified 99% of the landslides in the region could be triggered by antecedent rainfall of around 109 mm over a period of 15 days, indicating that the extreme rainfall events are becoming more frequent (Singh et al, 2025). There were 131 millimetres of rainfall during 1 day in Solan, in August 2023. The heavy and erratic rainfall during monsoon 2025 triggered the landslides in Garhwal Himalayas to a great magnitude due to the activation of long dormant landslide zones (Saha & Bera, 2026).

Most of the 340+ rural settlements in Solan are served by naulas or dharas (shallow wells and springs). Pit latrines, which are often built on hillslopes without the involvement of engineers, are the mainstay of sanitation systems. A disaster risk assessment in Rwanda indicates that more than 57 water and sanitation infrastructure sites have been affected by landslides, while Rwanda's overall resilience index was only 46% in 2025. In rural households, women make up more than 90% of the population and are at the greatest risk of adverse effects from service interruptions (Nepal et al., 2024). This is a common problem throughout the Himalayas.

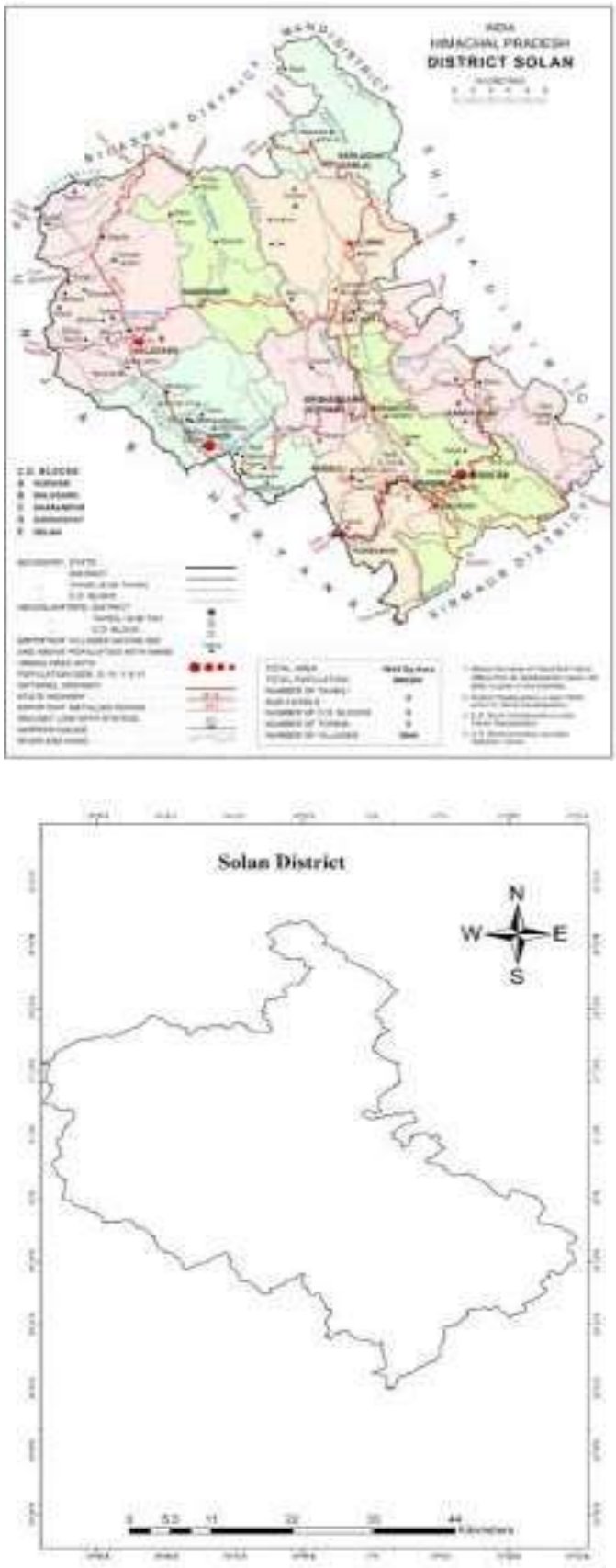

Figure 1: Location and administrative map of Solan district, Himachal Pradesh, India.

The district map of the Solan district, Himachal Pradesh, India, is displayed in figure 1.The district boundary line shown in red on the map is in the C.D. roads (including NH-5, state highways, a railway line, rivers and khads), important settlements (including Solan town), tahsil and sub-tahsil boundaries and blocks (Kunihar, Nalagarh, Dharampur, Kandaghat, Solan). The following important data are shown in the inset table: total area (1,916 km²), total population (580,320), number of tahsils (9), number of sub-tahsils (5), C.D. there are 2,644 villages, 6 towns, and 5 blocks. The latitude and longitude graticules can be seen at the edges.

3. Materials And Methods

3.1 Overall approach

The methodology followed was a three-step, cost effective approach: (1) collection of rainfall, SPI and TWI data, (2) comparison of index values at stable sites and landslides via logistic regression and quadratic discriminant analysis, and (3) overlaying maps of existing WASH infrastructure on areas with high TWI. All GIS operations were performed using the open-source software QGIS (version 3.34), as a way to demonstrate the results without the use of commercial software.

3.2 Data sources

Table 1 Summary of data sources, resolution, and cost.

Data	Source	Resolution	Cost
ALOS PALSAR DEM	Alaska Satellite Facility	12.5 m	Free
Landslide inventory	Bhukosh (GSI) via Magray et al. (2023)	214 point locations	Free
Annual Rainfall	India Meteorological Department (IMD)	0.25° grid	Free
WASH infrastructure points	District Water & Sanitation Mission (2024)	Springs, wells, latrines	Internal
Water quality data	District Health Office, Solan (2023)	Turbidity, coliform	Zenodo (doi:10.5281/zenodo.1299534)

3.3 TWI and SPI calculation

The computation of TWI and SPI are explained below.Standard terrain-analysis formulae were used to calculate TWI and SPI from the DEM:

- The formula TWI = ln(α / tan β) is input with the upslope contributing area per unit contour length (m2/m) and the slope angle (β) in radians. A high TWI indicates a landscape of gentle convergence that draws water.
- In this case, A_s is the particular catchment area, and SPI is equal to the natural logarithm of A_s divided by the tangent of λ. Surface runoff is concentrated in high SPI areas, particularly in convergent, steep areas.

In order to determine both indices, the 'Terrain Analysis' toolkit in QGIS was used. The usefulness of TWI in landslide susceptibility mapping has been demonstrated previously in the Mariana region of Brazil and Astore region of Pakistan (Usman, 2025; Xavier & Barella, 2024).

3.4 Sampling and statistical analysis

We documented the TWI, SPI and rainfall data for all 214 GSI landslide sites. 214 randomly located sites on level ground 100 metres or further from any landslide records were used as a control. Due to this separation, there was a decrease in autocorrelation within the spatial domain.

For each indicator separately, a binary logistic regression was performed to gauge the accuracy of TWI and SPI in predicting landslides. The analysis produced results, including coefficients, McFadden's pseudo R^2 and AUC. The same approach was adopted in China's Wuning region, and the same AUC value was obtained (Sun et al., 2024). Five-fold cross validation was used to assess model stability in the TWI logistic regression model and the mean area under the curve (AUC) with standard deviation was calculated. In addition, the additional value of TWI was evaluated using a basic slope-only logistic regression model, which used slope angle in degrees, and had an area under the curve (AUC) of 0.781.

Because any non-linearity between the landslide and non-landslide groups was considered possibly in each of the three predictors (TWI, SPI and rainfall), a quadratic discriminant analysis was performed in each of them.

3.5. Assessing Exposure of Water and Sanitation Infrastructure

GPS data were available for the District authorities for 1,912 pit latrines, 149 shallow wells and 240 communal springs. The optimised threshold from Youden's index (TWI > 6.2) was used to determine high-risk zones. The proportion of springs, wells and latrines in areas of high-TWI was calculated by overlying the locations of these infrastructure on the risk map.

The assessment of exposure is a smaller-scale version of a larger study released in 2024 by UNICEF and the Council on Energy, Environment and Water (CEEW) in a study that assessed the risks to India's WASH systems, posed by climate change. Districts are categorized into risk groups based on danger, exposure and susceptibility. Table 2 displays the results of the evaluation made in the Solan district.

Table 2 Climate-induced WASH risk assessment for Solan district, Himachal Pradesh

Risk component	Score	Category
Hazard	0.4049	Very high
Exposure	0.3722	Moderate
Vulnerability	0.2479	Low
Combined risk	0.0374	High

The Solan district falls under the very high hazard zone as it is part of the local landslide inventory, which means that the area is potentially affected by extreme climatic events like monsoon rainfall, flooding and landslides to a high degree or frequently. Moderate exposure on the district level; while it is physically hazardous, there is not a significant number of people or property directly at risk. The low vulnerability level means that the physical hazard is the main one that is driving the risk, not the socio-economic factors like poverty, access to healthcare, or infrastructure quality. High combined risk is underlined by the need for specific WASH adaptation measures for example low cost interventions (drainage clearance, latrine relocation, water quality emergency procedures) as highlighted in Section 5.2.

3.6 Cost estimation

A complete process replication was documented including the time and software cost. A WASH officer working in the district was expected to develop a TWI map and add WASH points using free software after a 2 day basic training in GIS. The total expense (Staff time, Basic laptop) would be less than **US$450 (approx. ₹43,000)**. The cost of a single damaged spring intake, which is sometimes more than $10,000 (or more than ₹10,00,000), makes this seem insignificant.

4. Results

4.1 Descriptive statistics

It is interesting to note that in Table 3 that landslide sites have a significantly higher TWI (Mean 5.86) and a considerably higher SPI (2.14) than the non-landslide sites (Mean 4.28 and 1.57 respectively). There was also higher rainfall at landslide locations (142 mm of average rainfall compared with 98 mm elsewhere).

Table 3 Summary statistics of TWI, SPI and rainfall at landslide vs. non-landslide points

Variable	Sample	Mean	Median	Std. Dev.	Min	Max
TWI	**Landslide**	5.86	5.72	1.14	3.02	10.34
	Non-landslide	4.28	4.15	1.02	1.76	8.91
SPI	**Landslide**	2.14	2.08	0.78	0.46	4.87
	Non-landslide	1.57	1.52	0.71	0.21	3.96
Annual Rainfall (mm)	**Landslide**	142.3	138.5	31.2	65.0	210.0
	Non-landslide	98.7	95.2	28.4	45.0	155.0

The TWI was significantly higher (mean 5.86 vs. 4.28) and the SPI was considerably higher (2.14 vs. 1.57) in landslide areas compared to non-landslide locations. The mean annual rainfall was also greater (142 mm per year), than in non-landslide areas (98 mm per year).

4.2 Logistic regression: TWI vs. SPI

Logistic regression analysis indicated that TWI was a very significant predictor ($p<0.001$) with AUC of 0.872, indicating that it has good discrimination power. Nevertheless, this was low (AUC = 0.764) for SPI. The fit was not improved (likelihood ratio test $p = 0.18$) when SPI was added to a TWI-only model. The results were consistent with those of a study on the Loess Plateau of China, which showed that the more factors that were added the worse the results were not always.

Table 4: Logistic regression performance of TWI and SPI

Metric	TWI	SPI

Coefficient (β_1)	0.2233	0.089
Pseudo-R^2 (McFadden)	0.7569	0.523
AUC (ROC)	0.872	0.764
AIC	384.2	468.9

Cross-validation:
The model was stable and validated by 5-fold cross validation of the logistic regression model of the model, the average AUC value of the logistic regression was 0.865 (±0.021)).
Threshold optimisation: Youden's index indicated that the best threshold for landslide prediction was TWI > 6.2, having a sensitivity of 0.84 and specificity of 0.81. The optimised threshold was used in the WASH exposure overlay as described in Section 4.4.
Slope-only comparison: The area under the curve (AUC) of a logistic regression model with only the slope angle (in degrees) was 0.781, far below the AUC of 0.872 for TWI. This is a testament to the fact that TWI can be used for more than just slope gradient for predictive data.

4.3 Quadratic discriminant analysis: TWI, SPI, and rainfall

TWI:
y = 0.3106x2 - 2.2233x + 2.5966 $R^2 = 0.7569$
SPI:
y = 0.3829x2 - 2.001x + 1.9841 $R^2 = 0.5094$
Annual Rainfall (annual total, mm):
y = -0.3151x2 + 2.0722x - 3.0363 $R^2 = 0.6596$

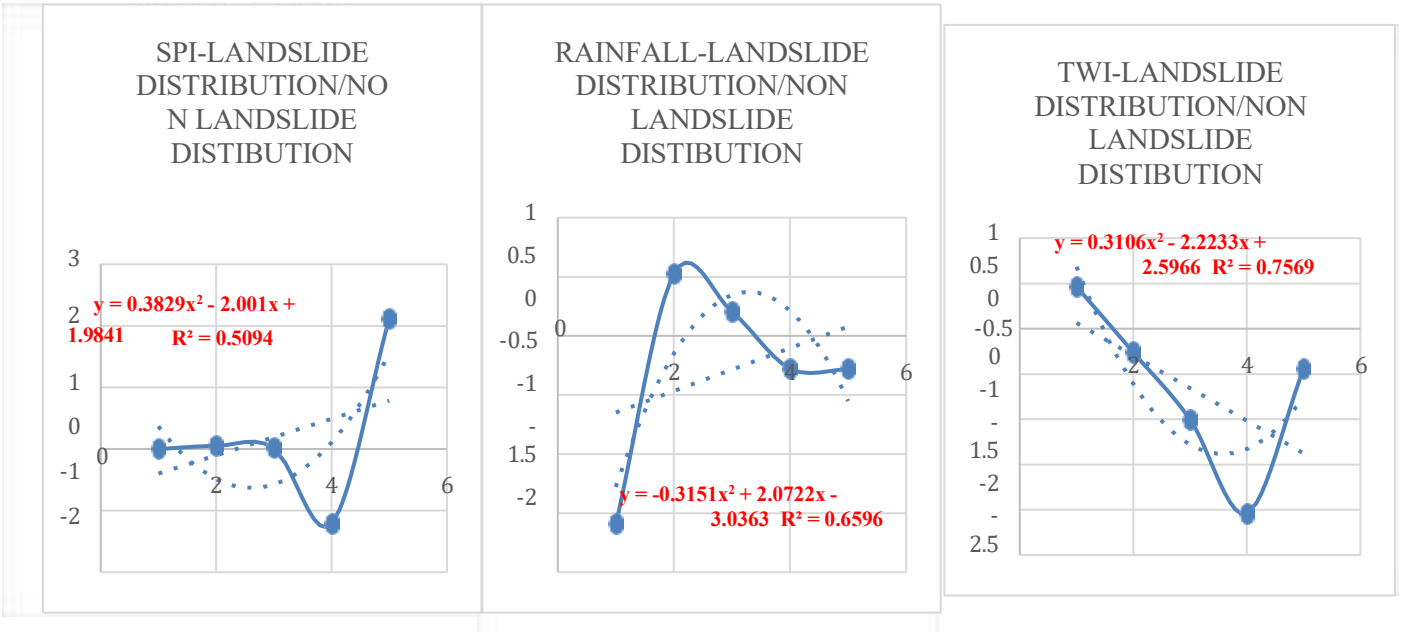

Figure 2 presents the fitted quadratic curves for the predictor, with equations and R^2 values.

- TWI was the strongest predictor with 75.7 % of the variation explained. For TWI values above approximately 5.5, the quadratic had a steep increase in the probability of landslides opening up.
- The rainfall accounted for 66.0% of the variation. Rainfall up to a certain magnitude (around 120-150 mm/day) was found to increase the landslide chance, while beyond this value, it was found to become less. This conclusion is in keeping with the idea that lengthy periods of rainfall and prior saturation of moisture are important factors.
- Stream power was also determined to have a secondary role in this clay dominated environment; the lowest was the variation explained by SPI was 50.9%.

4.4 WASH infrastructure exposure

Figure 3 shows the TWI map of the Solan area, which is based on the ALOS PALSAR DEM and is divided into five classes: 2.73-5, 5.01-8, 8.01-12, 12.01-16, and 16.01-23.72. The most extreme classes (TWI>8) are associated with the valley bottoms and convergent hillslope hollows where water accumulates. All 214 landslide locations are shown as black circles, indicating that there is a significant clustering at high total wave intensities (TWI).

The optimized threshold TWI> 6.2 (from Youden's index) was applied and the WASH infrastructure points was overlaid on the TWI raster, this indicated that most water sources are found in high TWI areas. Specifically, 78% of the springs (187/240) and 75% of the wells (106/149) are located in areas where TWI > 6.2. Table 5 shows that out of 1,912 pit latrines, 1,243 (or 65%) were used. These results show that communities have traditionally sited their water and sanitation systems in areas prone to landslides caused by saturation.

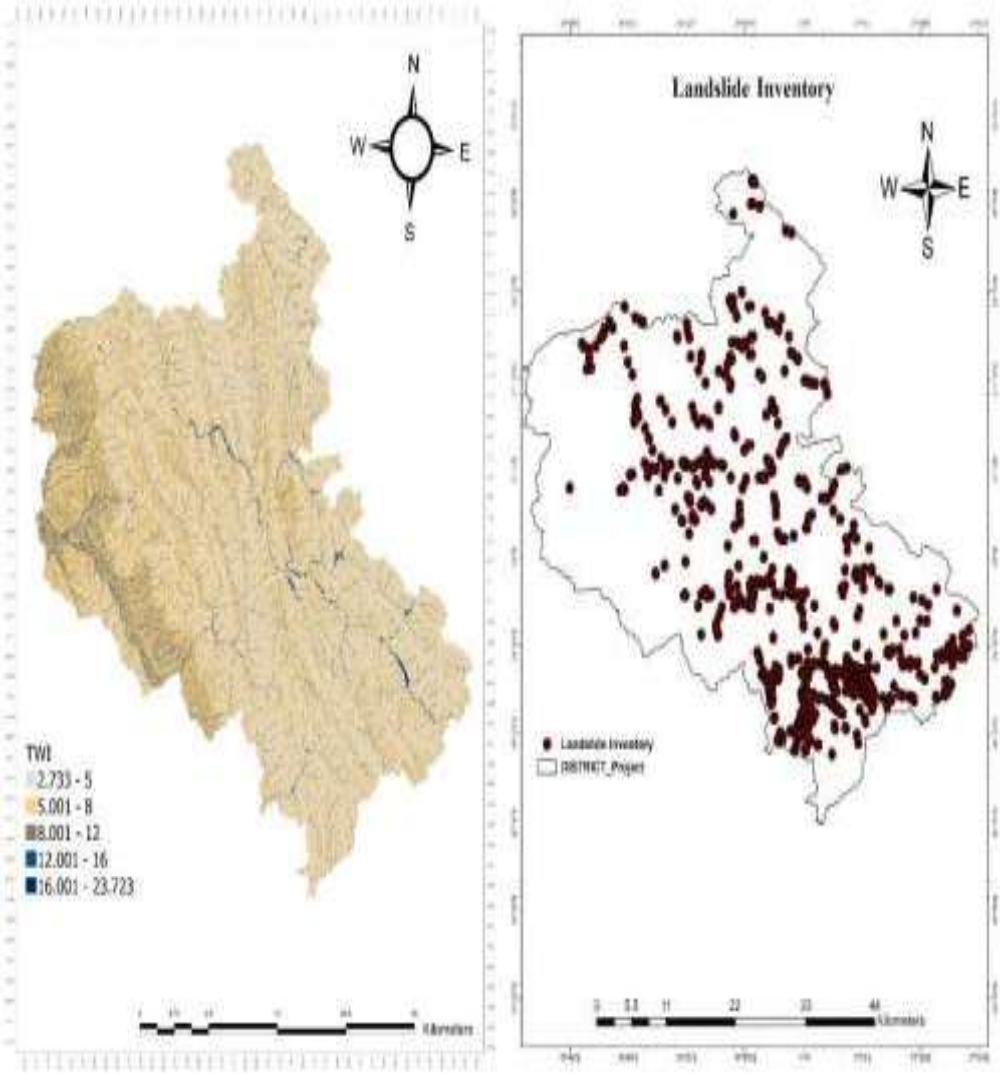

Figure 3. Topographic Wetness Index (TWI) map of Solan district with landslide points (n=214). TWI derived from ALOS PALSAR DEM (12.5 m) and classified into five intervals (2.73–5, 5.01–8, 8.01–12, 12.01–16, 16.01–23.72). Higher TWI (darker red) indicates convergent, poorly drained areas prone to saturation and landsliding. Black circles represent the 214 inventoried landslide points (GSI Bhukosh). High-resolution image (300 DPI) with scale bar (0–38 km) and north arrow.

Table 3 WASH infrastructure located within high-TWI zones (TWI > 6.2)

Infrastructure	Total number	Number in high-TWI	% exposed
Springs	240	187	**78%**
Shallow wells	149	106	**71%**
Pit latrines	1,912	1,243	**65%**

4.5 Water quality impacts of a landslide event

After the heavy rains in August 2023, a landslide blocked the intake of a spring-fed piped system that supplied water to three villages. The water quality in the area was severely degraded, as reflected in Table 6, based on the information gathered by the District Health Office and published in Zenodo (doi:10.5281/zenodo.1299534).

Table 4 Water quality deterioration after a landslide event (August 2023, n=12 springs).

Parameter	Before landslide (mean)	After landslide (mean)	Change
Turbidity (NTU)	3.2	14.7	**+359%**
Coliform (MPN/100 mL)	<10	>500	**>50× increase**

5. Discussion

5.1 Why TWI outperformed rainfall and SPI

In both logistic and quadratic models, the probability of landslides in Solan was highly predicted by TWI. Saturation-driven failure of the clayey Siwalik is the most frequent type of failure. This failure is characterized by the presence of water in convergent hollows (high TWI) that leads to an increase in pore pressure which, in turn, leads to failure and eventual collapse without erosion of the surface. The ingredients in conglomerates are cemented by a red clay in the Siwalik zone of Nepal. These materials will weather and turn loose and brittle. As per Bhandari and Dhakal (2018) the causative factor of the landsliding is the presence of heavily weathered mudstone beds.

Although rainfall is a significant factor, it only accounted for 66% of the variation in the data. This is because the same amount of rain can affect different areas in different ways, depending on the local topography. An strong localised rainfall event in August 2025 caused a chain reaction of mudslides, flash floods, and floods, resulting in the destruction of more than 148 structures in the Dharali tragedy (Sharma & Sati, 2026). The poor performance of 51% of SPI tests indicated that in this instance it was not stream power that was the primary driver. The TWI and SPI were found to be two of the thirteen potential causes by research done in the Chamoli Himalayas, and frequency ratio models were developed with an area under the curve (AUC) of 0.923 (Bharadwaj & Sarkar, 2024). Furthermore, the ability of TWI to detect hydrological events that were not detected by basic slope gradient indicates that basic slope gradient was able to achieve an AUC of only 0.781.

This is a clear implication of practice that monitoring rainfall is vital to estimating the risks to WASH infrastructure from landslides, and mapping water flows (TWI) is even more essential.

5.2 Practical implications for WASH programming

Relevance of WASH programs in practical terms

The exposure study (Table 5) confirmed that more than 70% of wells and springs are in areas where there is high total water input (TWI). Identified were three treatments with minimal costs and significant impacts:

1. TWI-based risk mapping as a technique for regular planning. A TWI map can be created in a few hours for each district that has a DEM. This map is meant to be used for pre-monsoon maintenance and should be reviewed prior to building new water stations or latrines. Some of the assessments can be further simplified by adopting open-source softwares, e.g., the QGIS Geohazard plugin (Castelli et al., 2025).
2. In the high TWI areas, the care of waterways had to be done in advance of the monsoon. You may lessen the amount of water that collects near springs and wells by unclogging drains, lining culverts and building little check dams. Bhandari and Dhakal (2018) have observed that reducing soil saturation is the key to minimising landslides in Siwalik zone.
3. Separating restrooms from areas where pesticides are used and spilt. Pit latrines in high total wastewater input (TTWI) areas pose a great risk of collapse and if damaged, can become sources of faeces pollution. Children in Nepal are affected by diarrhoea, coughing, fever as a result of the lack of personal cleanliness due to the covering of toilets by landslides (Nepal et al., 2024).

4. Emergency procedure on water quality following a landslide. The basic flowchart can be referred to by the District authorities as follows: (a) any landslide in the high-TWI zone is the trigger; (b) immediate actions are a 24-hour turbidity test, chlorination of all affected springs and a public health notice; (c) follow-up actions are weekly coliform testing for four weeks and repair work on damaged intakes. The results of the water quality analysis in Table 6 are immediately put into practice by following this approach.

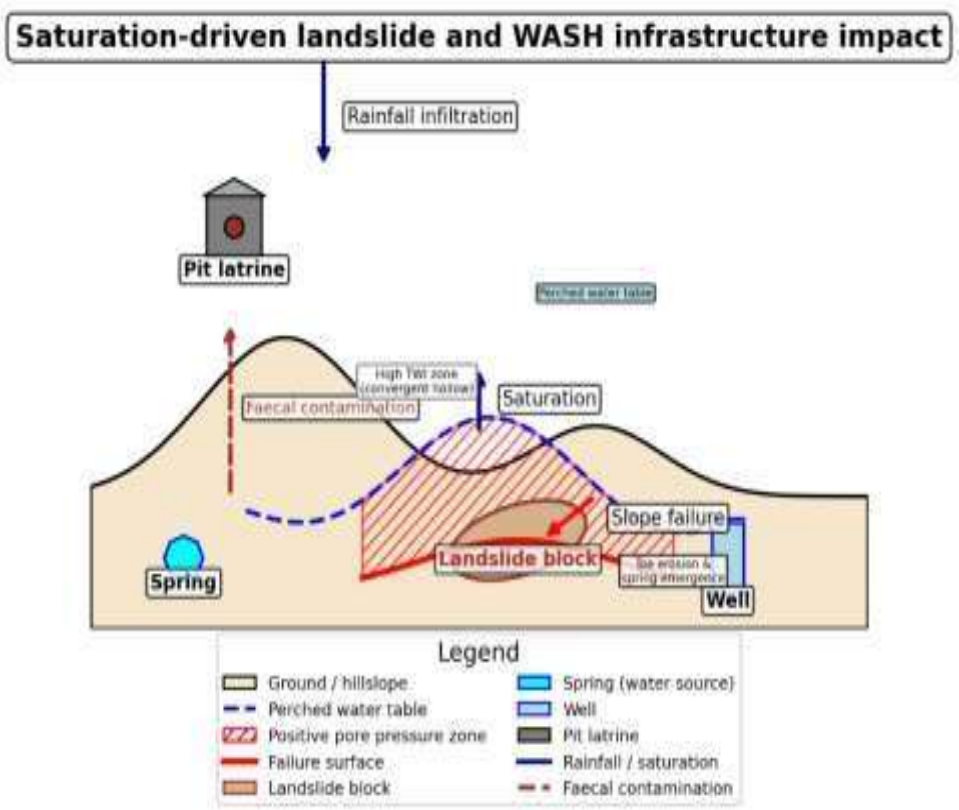

Figure 5. Schematic diagram of a saturation-driven landslide and its impact on water supply and sanitation (WASH) infrastructure. The diagram illustrates a hillslope with a convergent hollow (high TWI zone), a perched water table, a zone of positive pore pressure, a failure surface, and a displaced landslide block. An uphill pit latrine
releases fecal contamination that flows along the landslide scar, contaminating the spring and well at the toe. Arrows indicate rainfall infiltration, soil saturation, slope failure, and the contamination pathway.

5.3 Replicability and cost

The entire analysis used free data (ALOS PALSAR DEM, IMD rainfall, open landslide inventory) and open-source QGIS. At typical development-sector salary levels, staff time (3–5 days for a trained analyst) amounted to **<US$500 (approx. ₹43,000)**. This is trivial compared to the cost of a single destroyed spring intake (often >US$10,000, i.e., >₹10,00,000). The QGIS-FORM plugin, validated using the 2022 Maerkang landslide event, demonstrates how open-source probabilistic modelling can produce reliable landslide susceptibility maps (Zhang et al., 2024). State disaster management authorities should include TWI maps in their pre-monsoon WASH infrastructure risk assessments.

5.4 Limitations and future directions

The assessment was conducted with open-source QGIS software and free data such as ALOS PALSAR DEM, IMD rainfall, and open landslide inventory. When workers' time at the usual compensation ranges in the development industry (three to five days for certified analyst), time spent is approximately $43,000 (<US$500). This is a minor cost in comparison to the cost of a single damaged spring intake (which can cost more than $10,000 or more than ₹10,00,000). Zhang et al. (2024) verified the QGIS-FORM plugin using the Maerkang landslide event of 2022, which shows how open-source probabilistic modelling can provide trustworthy landslide susceptibility maps. State DMAs need to consider the risk to WASH infrastructure prior to the onset of the monsoon, incorporating TWI maps.

6. Conclusions

In this research, the scientists discovered the Topographic Wetness Index (TWI) was useful in identifying which water and sanitation systems in rural areas in the Himalayas were vulnerable to landslides. TWI alone accounted

for 75.7% of landslide incidence when considered separately from rainfall (which accounted for 66.0%), and was more than the Stream Power Index (50.9%). After five-fold cross validation, the model proved to be stable (with a mean AUC of 0.865) and logistic regression model gave good results with AUC = 0.872. On the other hand, a slope-only model was only able to achieve an AUC of 0.781, demonstrating that TWI reflects the unique hydrological processes. Using the optimised threshold TWI > 6.2, 71% of wells and 78% of springs fell into high-TWI zones, indicating that they are extremely vulnerable to saturation-driven slope collapses, when the TWI map was superimposed with the local infrastructure. Water quality was drastically affected following a landslide, with turbidity up 359% and coliform counts over 50 times the normal level, which is a potential risk to health.

For all those working in WASH - water, sanitation, hygiene, the risk of landslides should be an accepted element of the design and protection of drinking water sources. With the use of free software and a few days of staff training, a TWI map may be made for less than $500 (about ₹43,000). Once the map is ready the following actions become more apparent; remove debris from drains in areas of high total rainfall intensity (TWI), move the latrines away from areas of high TWI, do not construct new infrastructure on high TWI areas, and implement a policy of emergency water quality post landslide. The impact of these inexpensive actions may be substantial. This kind of cost-effective measure is now a must, given the increased and erratic rainfall in the Himalayas due to climate change.

Acknowledgments

The authors would like to thank the following organizations: Geological Survey of India (GSI) for the support provided for maintaining Bhukosh Portal, the India Meteorological Department for rainfall data, the Alaska Satellite Facility for providing open access ALOS PALSAR DEM data and the Solan District Water & Sanitation Mission and District Health Office for providing data on WASH infrastructure and water quality post landslide. The water quality records are donated to Zenodo with the DOI 10.5281/zenodo.1299534. There was no outside funding for this project. Section 4.5 was completed with the oral informed consent of the resident.

References

1. Beven, K. J., & Kirkby, M. J. (1979). A physically based, variable contributing area model of basin hydrology. Hydrological Sciences Bulletin, 24(1), 43–69.
2. Bhandari, B. P., & Dhakal, S. (2018). Lithological control on landslide in the Babai Khola watershed, Siwaliks zone of Nepal. American Journal of Earth Sciences, 5(3), 54–64.
3. Bhandari, B. P., & Dhakal, S. (2020). Compositional analysis and phase relations of soil mass from the active landslides o f Babai River watershed, Siwalik zone of Nepal. Engineering Geology, 105851.
4. Bharadwaj, D., & Sarkar, R. (2024). Landslide susceptibility mapping using probabilistic frequency ratio and Shannon entropy for Chamoli, Uttarakhand Himalayas. Iranian Journal of Science and Technology, Transactions of Civil Engineering, 48(1), 377–395.
5. Castelli, M., Filipello, A., Fasciano, C., et al. (2025). Geohazard Plugin: A QGIS plugin for the preliminary analysis of landslides at medium–small scale. MDPI AG.
6. Chandna, P., Kumar, G., & Sarkar, S. (2026). Quantifying antecedent rainfall effects on landslides in the Garhwal Himalayas. EGU General Assembly 2026, EGU26-18511.
7. District Water & Sanitation Mission, Solan. (2024). Annual report on rural water supply and sanitation infrastructure. Government of Himachal Pradesh.
8. Froude, M. J., & Petley, D. N. (2018). Global fatal landslide occurrence from 2004 to 2016. Natural Hazards and Earth System Sciences, 18(8), 2161–2181.
9. Gu, Z., Yao, X., Yao, C., & Li, C. (2021). Applicability of geomorphic index for the potential slope instability in the Three River Region, Eastern Tibetan Plateau. Sensors, 21(19), 6505.
10. IFRC. (2023). Landslides: Damage to health facilities and WASH infrastructure. Epidemics.
11. India Meteorological Department. (2023-2024). Gridded rainfall data (0.25°). Pune, India.
12. INSEC. (2024). Residents suffer due to unrepaired water source damaged by landslide. INSEC Online, 2 October 2024.
13. Magray, A. A., Singh, K., & Sharma, S. (2023). Comparative analysis of certainty factor and analytic hierarchy process for landslide susceptibility zonation in parts of Solan, Himachal Pradesh, India. Quaestiones

Geographicae, 42(3), 5–18.

14. Monga, D., & Ganguli, P. (2025). Developing site-specific rainfall thresholds for landslide prediction in the Himalayas: A comparative assessment between Northwestern and Northeastern Himalayas. EGU General Assembly 2025, EGU25-7120.
15. Moore, I. D., Grayson, R. B., & Ladson, A. R. (1991). Digital terrain modelling: A review of hydrological, geomorphological, and biological applications. Hydrological Processes, 5(1), 3–30.
16. Nepal, S., Aryal, A., Karki, D., & Koirala, S. (2024). Addressing climate vulnerability in Nepal through resilient inclusive WASH systems (RES-WASH). International Water Management Institute (IWMI), Kathmandu.
17. Republic of Rwanda Ministry in charge of Emergency Management. (2025). Disaster risk mitigation plan for water and sanitation sector Kigali, Rwanda.
18. Saha, S., & Bera, B. (2026). Preliminary assessment of heavy rainfall-induced landslides and reactivation of old landslides in the Garhwal Himalayas. Landslides, Springer Nature.
19. Sangeeta & Singh, S. K. (2023). Influence of anthropogenic activities on landslide susceptibility: A case study in Solan district, Himachal Pradesh, India. Journal of Mountain Science, 20(2), 429–447.
20. Sharma, S., & Sati, S. P. (2026). The Dharali debris flow flood: Warning from the Himalaya. Journal of Geological Society of India, 102(5), 718–722.
21. Singh, J., Thakur, M., Dhiman, R. K., et al. (2025). Development of rainfall threshold equation and bayesian probabilistic analysis for landslide prediction: A case study of Shimla, Northwestern Himalaya, India. Natural Hazards Research, 5(3), 455–467.
22. Sun, D., Wang, J., Wen, H., Ding, Y., & Mi, C. (2024). Comparison of DL, SVM and LR models for landslide susceptibility mapping. Journal of Rock Mechanics and Geotechnical Engineering, 8, 3221–3232.
23. The Tribune. (2025). Rains of ruin: Solan reels under a deluge of despair. The Tribune India, 7 September 2025.
24. The Tribune. (2026). Climate change, human activities fuel landslide risks in Himachal: Experts. The Tribune India, 15 March 2026.
25. UN General Assembly. (2010). Resolution 64/292: The human right to water and sanitation.
26. UNICEF. (2025). Prioritising good sanitation and hygiene in the aftermath of landslides. UNICEF China, 16 September 2025.
27. Usman, M. (2025). GIS-based landslide susceptibility mapping using analytical hierarchy process: A case study of Astore region, Pakistan. Geoscientists Society GB.
28. Xavier, M. O., & Barella, C. F. (2024). Landslide susceptibility mapping using logistic regression, random forests, and artificial neural networks: A case study in Mariana/MG, Brazil. Brazilian Journal of Geomorphology, 25(4).
29. Zhang, L., et al. (2024). A QGIS framework for physically-based probabilistic modelling of landslide susceptibility: QGIS-FORM. Environmental Modelling & Software, 106258.
30. Bhattarai, P., & Kafle, G. (2021). Role of geological structures and clay minerals in the occurrence of landslides along Mugling-Narayanghat Highway section. TUCL Repository.
31. Bera, A., Mukhopadhyay, B. P., & Das, D. (2024). Landslide susceptibility mapping using morphological and hydrological parameters in Sikkim Himalaya. Natural Hazards, 120(3), 2145–2172.
32. Bisht, S., Rawat, G. S., & Tiwari, A. (2023). Landslide susceptibility prediction using frequency ratio model: A case study of Uttarakhand, Himalaya (India). Environmental Earth Sciences, 82(1), 34.
33. Crosta, G. B., & Frattini, P. (2008). Rainfall-induced landslides and debris flows. Hydrological Processes, 22(4), 489–501.
34. Guzzetti, F., Peruccacci, S., Rossi, M., & Stark, C. P. (2008). The rainfall intensity–duration control of shallow landslides and debris flows: An update. Landslides, 5(1), 3–17.
35. Sidle, R. C., & Bogaard, T. A. (2016). Dynamic earth system and ecological controls of rainfall-initiated landslides. Earth-Science Reviews, 159, 275–291.

36. Tofi, M. (2025). Using drone-based multispectral imaging for investigating gravelly debris flows and geomorphic characteristics. Environmental Earth Sciences, 83, 247.
37. Borga, M., Fontana, G. D., & De Ros, D. (2002). Analysis of topographic and climatic controls on rainfall-triggered shallow landsliding. Natural Hazards and Earth System Sciences, 2(3/4), 181–189.
38. UNICEF and Council on Energy, Environment and Water (CEEW) (2024). *Assessing Risks to India's Drinking Water, Sanitation, and Hygiene Systems from Extreme Climate Events*. Available at: ceew.in (accessed June 2025).